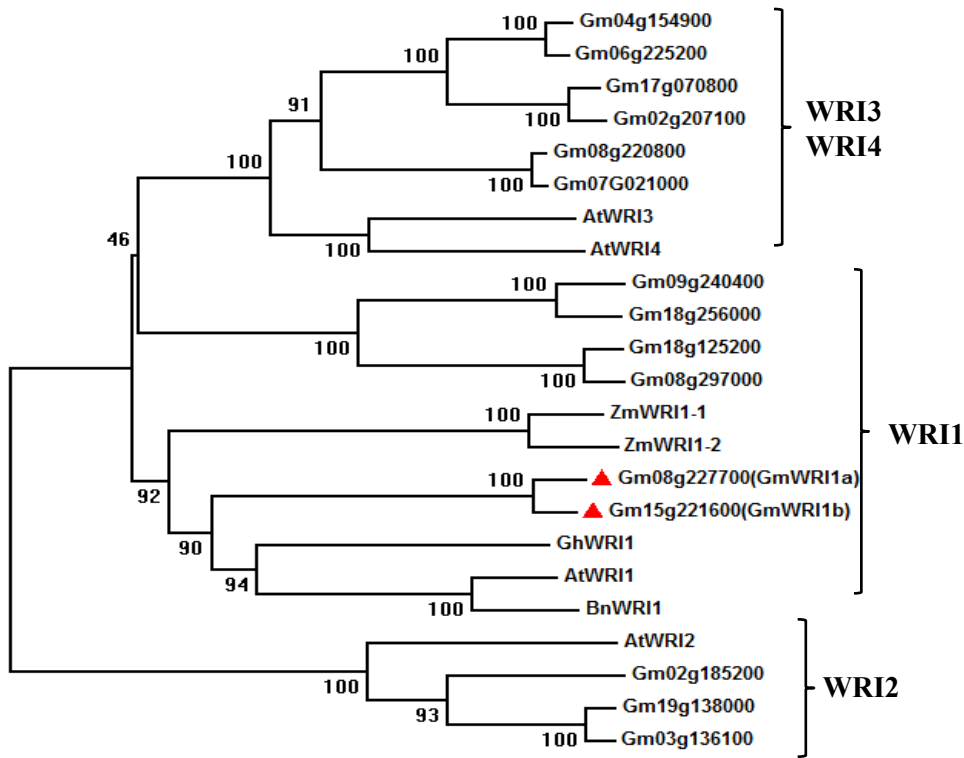
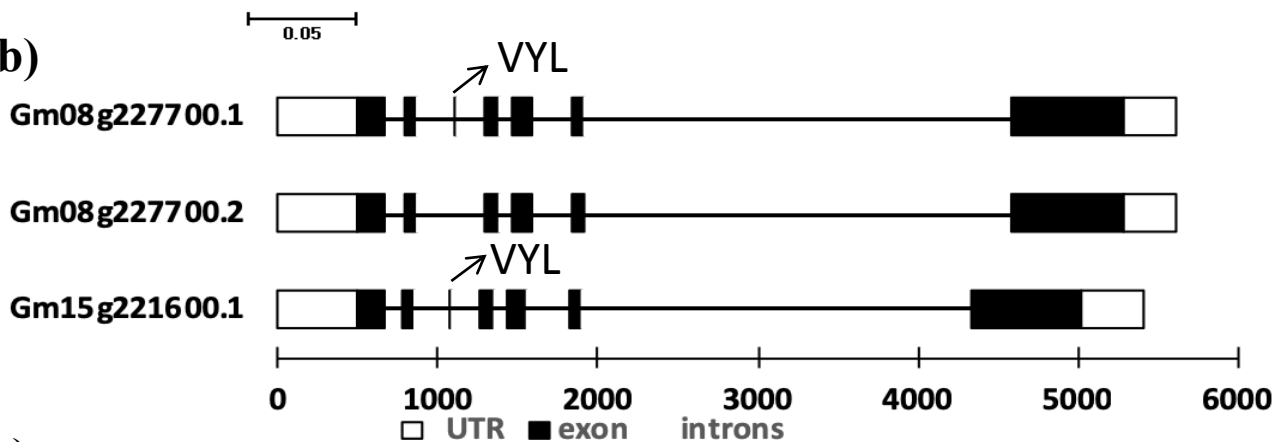


Figure S1

(a)



(b)



(c)

Gm08g.1 : MKRSPASSCSSSTSSVGFVHHPIEKRRPKHPRRNLLKSQKCKQNQTTTGGRRSSIYRGVTRHRWTGRFEAHLWDKSSWNNIQSKKGQVYLGA YDTEESAARTYDI : 107
 Gm08g.2 : MKRSPASSCSSSTSSVGFVHHPIEKRRPKHPRRNLLKSQKCKQNQTTTGGRRSSIYRGVTRHRWTGRFEAHLWDKSSWNNIQSKKGQ---GAYDTEESAARTYDI : 104
 Gm15g.1 : MKRSPASSCSSSTSSVGFEA--PIEKRRPKHPRRNLLKSQKCKQNQTTTGGRRSSIYRGVTRHRWTGRFEAHLWDKSSWNNIQSKKGQVYLGA YDTEESAARTYDI : 105

Gm08g.1 : AALKYWGDATLNFPIETYTKLEEMDKVSREEYLASLRQSSGFSRGISKYRGVARHHHNGRWEARIGRVCNGKYLGLTYKTQEEAAVAYDMAAIEYRGVNAVITM : 214
 Gm08g.2 : AALKYWGDATLNFPIETYTKLEEMDKVSREEYLASLRQSSGFSRGISKYRGVARHHHNGRWEARIGRVCNGKYLGLTYKTQEEAAVAYDMAAIEYRGVNAVITM : 211
 Gm15g.1 : AALKYWGDATLNFPIETYTKLEEMDKVSREEYLASLRQSSGFSRGLSKYRGVARHHHNGRWEARIGRVCNGKYLGLTYKTQEEAAVAYDMAAIEYRGVNAVITM : 212

Gm08g.1 : FDISNYMDKIKKKNDQTLQQCQTEVQTETVPNSSDSEEA EVEQCHTTTITPPPSLENLHMLPQEHQVQYTHHVTPRDEESSSLVTIMEHVLEQDLPWSEFMYTGLSQF : 321
 Gm08g.2 : FDISNYMDKIKKKNDQTLQQCQTEVQTETVPNSSDSEEA EVEQCHTTTITPPPSLENLHMLPQEHQVQYTHHVTPRDEESSSLVTIMEHVLEQDLPWSEFMYTGLSQF : 318
 Gm15g.1 : FDISNYMDKIKKKNDQT-QCQCTEAQTETVPNSSDSEEA EVEQC---TTTITPPPSLENLHMLPQCHQVQYTPHVSPRDEESSSLITIMHVLEQDLPWSEFMYTGLSQF : 317

Gm08g.1 : QDPNLALSKGDDDLVGMFESAGFEEDIDFLFSTQPGIHE TESDVNNMSAVLDSVECGDTNGAGGRSMVYHVHDN NNKQKRLMSFASSSSPSTTTTVSCDYALDI : 426
 Gm08g.2 : QDPNLALSKGDDDLVGMFESAGFEEDIDFLFSTQPGIHE TESDVNNMSAVLDSVECGDTNGAGGRSMVYHVHDN NNKQKRLMSFASSSSPSTTTTVSCDYALDI : 423
 Gm15g.1 : QDPNLAFCKGDDDLVGMFESAGFEEDIDFLFSTQPGIHE TESDVNNMSAVLDSVECGDTNGAGG---SMMHVDN---KQKIVSFASSP---SSTTTVSCDYALDI : 412

Figure S1. Phylogenetic (a) and gene structure analysis (b) and protein sequence alignment (c) of GmWRI1s.

(a) Unrooted phylogenetic tree of WRINKLED1s (WRI1) from various plants. The alignment was generated using Clustal and the unrooted phylogram was constructed with MEGA6 software using the neighbor-joining method, with bootstrap values based on 1000 replicates.

Figure S2

(a)

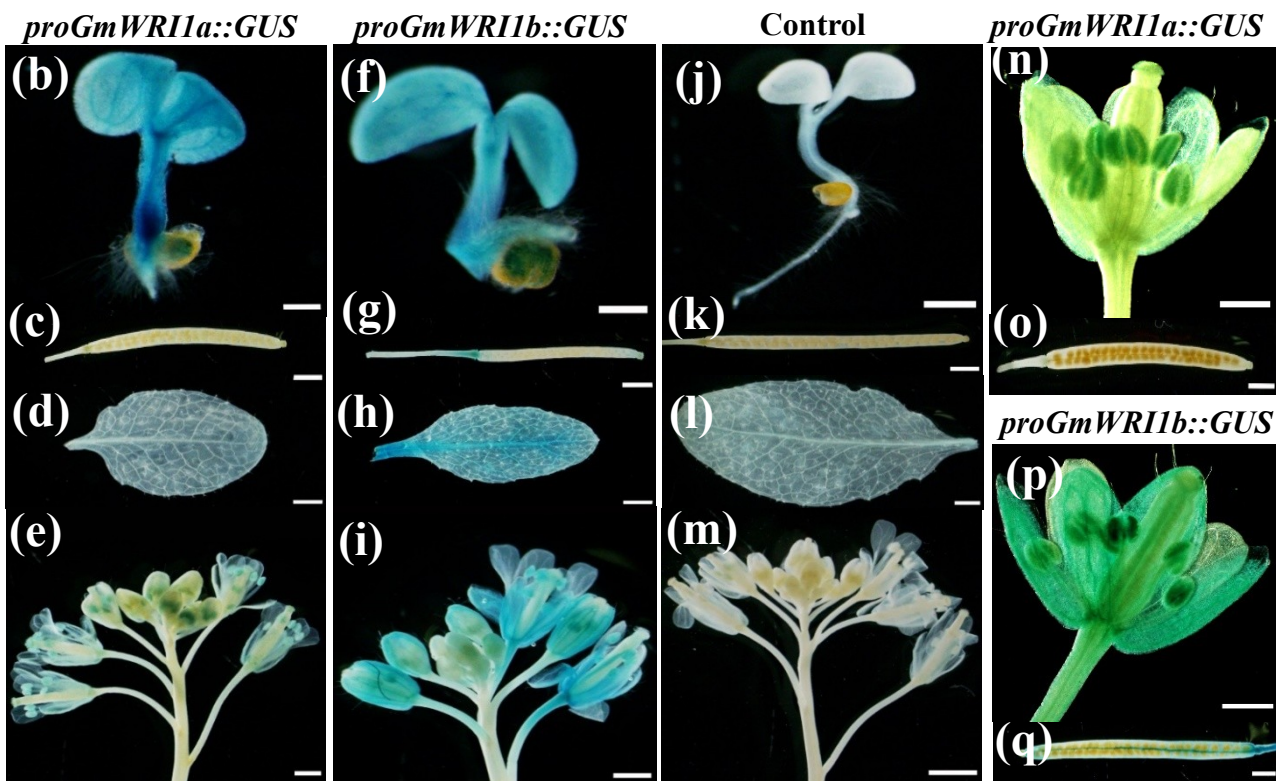
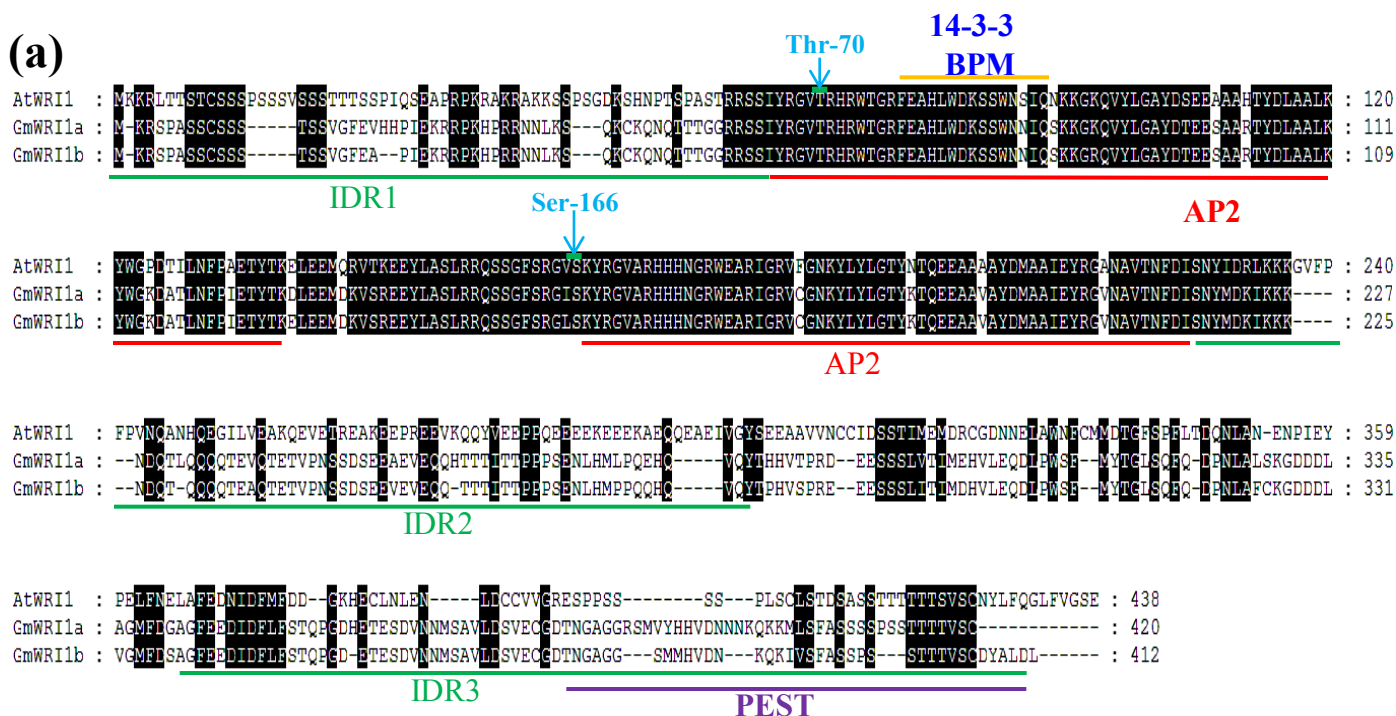


Figure S2. Schematic diagram of the GmWRI1s and AtWRI1 predicted protein sequence illustrating the locations of known domains.

(a) The two AP2 DNA binding domains are shown in red; three intrinsically disordered regions (IDR) are shown in green line. Two KIN10 phosphorylation sites are shown as blue bars. The 14-3-3 phosphopeptide binding site and BPM binding site colocalize to the same region represented by an orange line. The C-terminal PEST domain, residues with in IDR3, is represented as a purple line.

(b-e, o,p) Distribution of GUS activities in *proGmWRI1a::GUS* Arabidopsis plants.

(f-i, p,q) Distribution of GUS activities in *proGmWRI1b::GUS* Arabidopsis plants.

(j-m) Distribution of GUS activities in wild-type control plants.

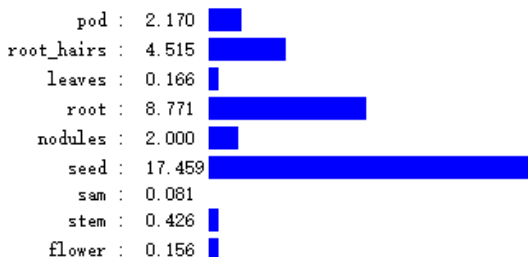
Histochemical detection of GUS activity in different tissues, including seedling (b, f, j), young pod (c, g, k), leaf (d, h, l), inflorescences (e, i, m), flower (n, p), and old pod (o, q). Bars=500µm in (b), (f), (j) and (e, i, m), 1mm in pod, leaf and 50µm in flower.

Figure S3

(a)

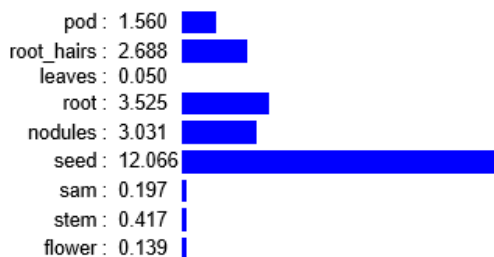
Glyma.08G227700.1 Nine Tissue Transcript-level Expression

FPKM Coefficient of variance: 1.460
(across samples below)



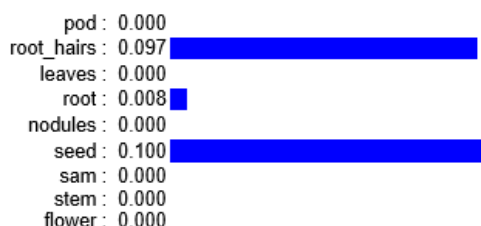
Glyma.15G221600.1 Nine Tissue Transcript-level Expression

FPKM Coefficient of variance: 1.440
(across samples below)



Glyma.08G227700.2 Nine Tissue Transcript-level Expression

FPKM Coefficient of variance: 1.889
(across samples below)



Note: CuffDiff run status is displayed in the rightmost column if reported as other than OK for one or more samples.

(b)

From resource file Table_S5.csv ([download resource file](#))

Raw Data: digital gene expression counts of the uniquely mappable reads.

Download List	young_leaf	flower	one cm pod	pod shell 10DAF	pod shell 14DAF	seed 10DAF	seed 14DAF	seed 21DAF	seed 25DAF	seed 28DAF	seed 35DAF	seed 42DAF	root	nodule
Glyma08g24420	3	0	1	2	0	5	34	44	112	63	133	37	24	6
Glyma15g34770	11	1	1	1	0	14	42	26	108	60	125	27	30	21

Figure S3. Public data for expression of soybean GmWRI1s

(a) Expression patterns of GmWRI1 in different tissues of soybean plant. The public data are shown in phytozome (<https://phytozome.jgi.doe.gov/>). *GmWRI1a* (Glyma08g227700.1 in v10, Glyma08g24420 in v9), *GmWRI1a'* (Glyma08g227700.2 in v10), *GmWRI1b* (Glyma15g221600.1 in v10, Glyma15g34770 in v9). (b) *GmWRI1* mainly expressed in developing seeds. These data are retrieved from soyKB (www.SoyKB.com)

Figure S4

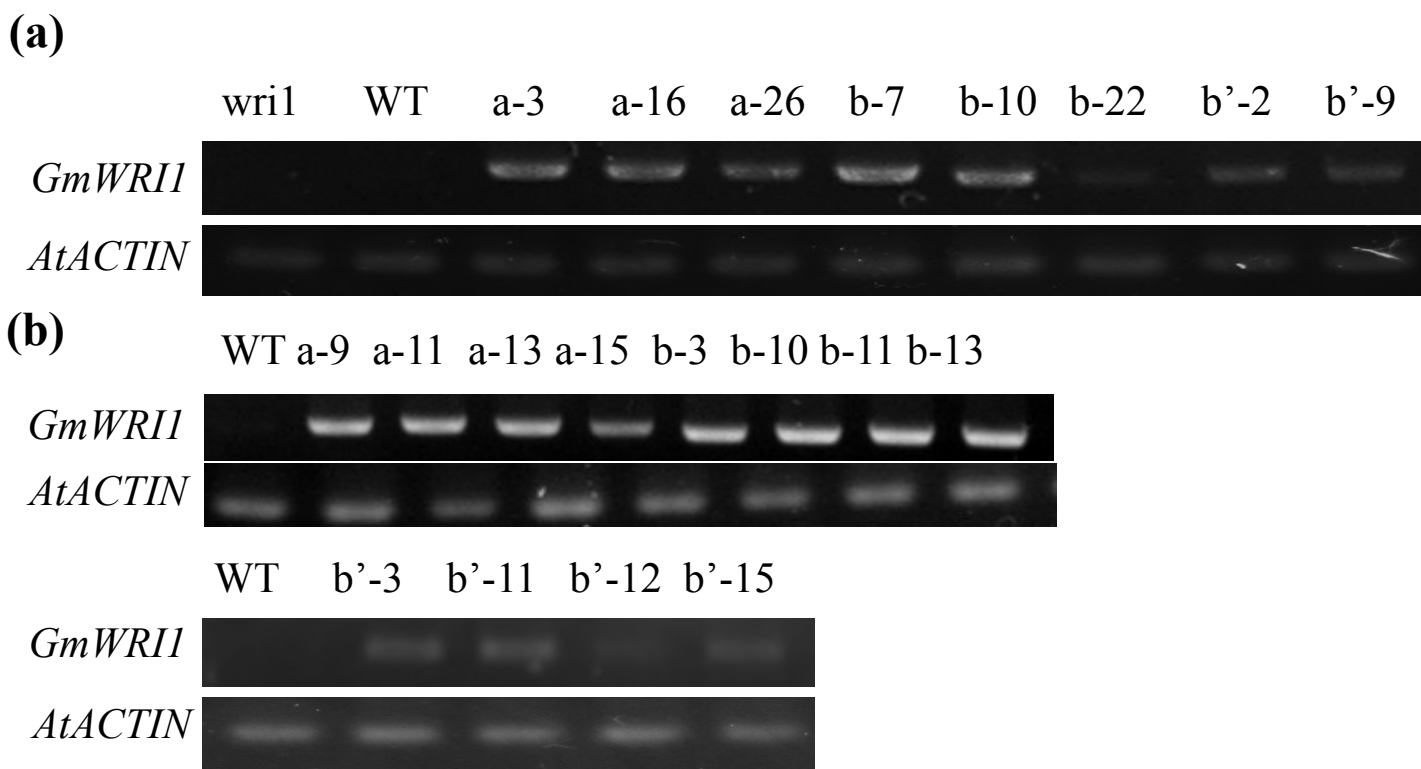


Figure S4. Confirmation of transgenic *atwri1-1* (a) and wild-type (b) plants over-expressing *GmWRI1*s.

Figure S5

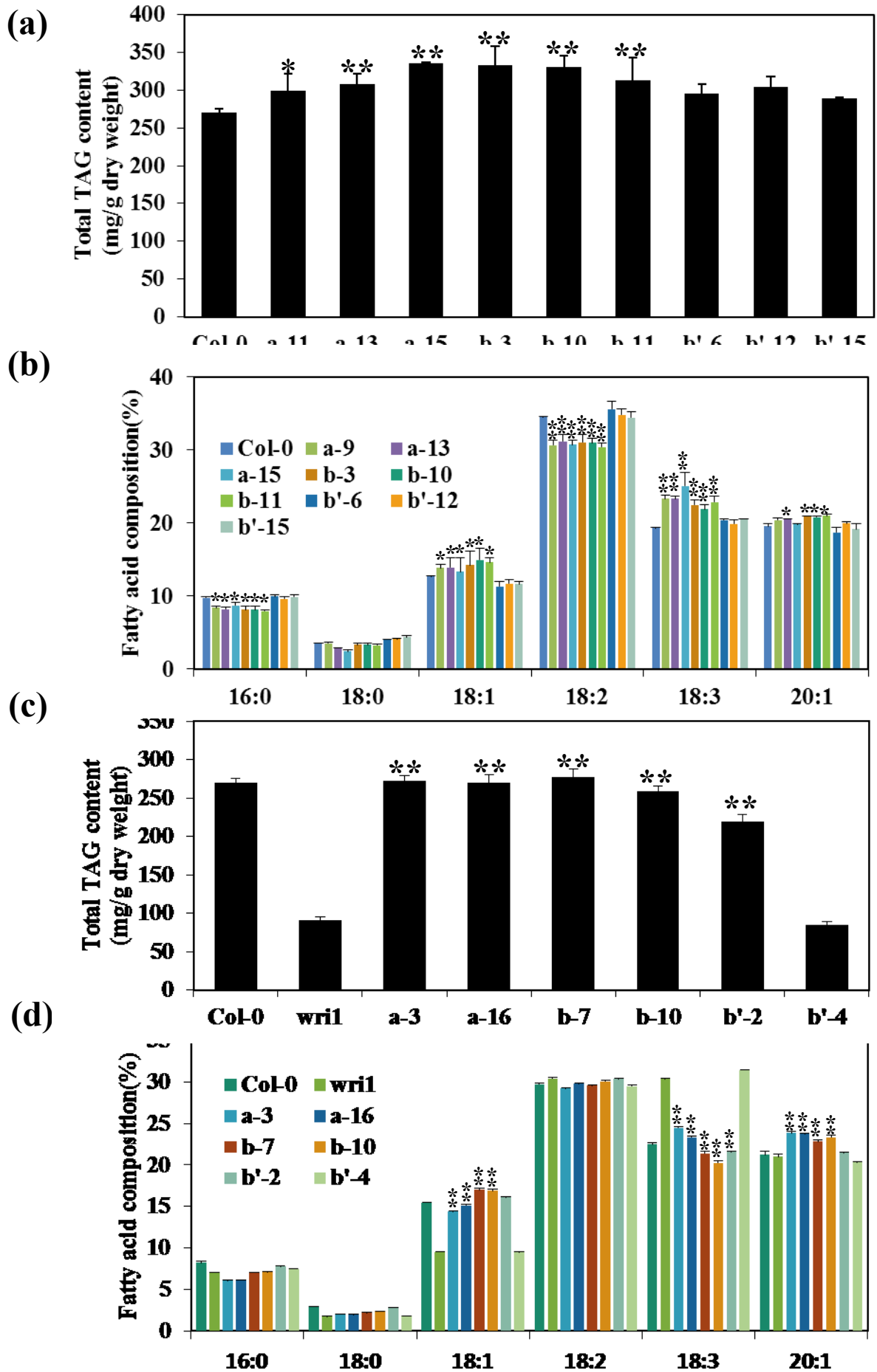


Figure S5. Functional expression of *GmWRI1a* and *b* in *Arabidopsis thaliana* seeds

(a) Total TAG contents in *GmWRI1s* expressing *Arabidopsis* seeds.

(b) Fatty acid composition in TAGs from wild-type *Arabidopsis* seeds expressing *GmWRI1s*

(c) Total TAG contents in *GmWRI1s*-complemented *Arabidopsis wri1-1* mutant seeds

(d) Fatty acid composition in TAGs from *Arabidopsis atwri1-1* mutant seeds expressing *GmWRI1s*

All data are expressed as mean \pm SD from at least three biological duplicates. * $P < 0.05$ and ** $P < 0.01$ by Student's *t* test for significant difference. T3 transgenic *Arabidopsis* seeds were used for analysis.

Figure S6

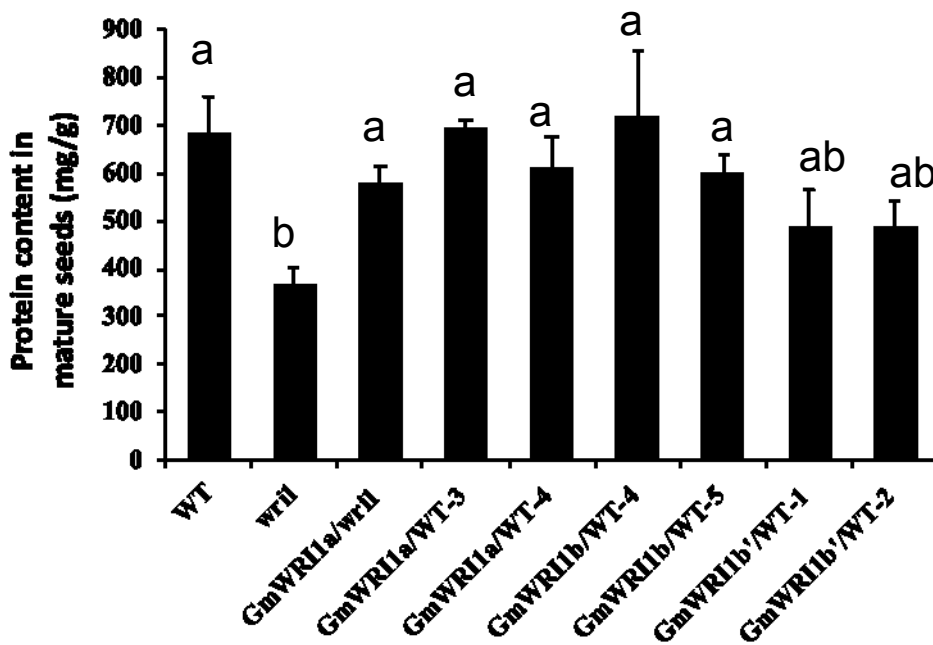


Figure S6. Proteins content of wild type, *atwri1* mutant and transgenic plant in mature seeds.

Figure S7

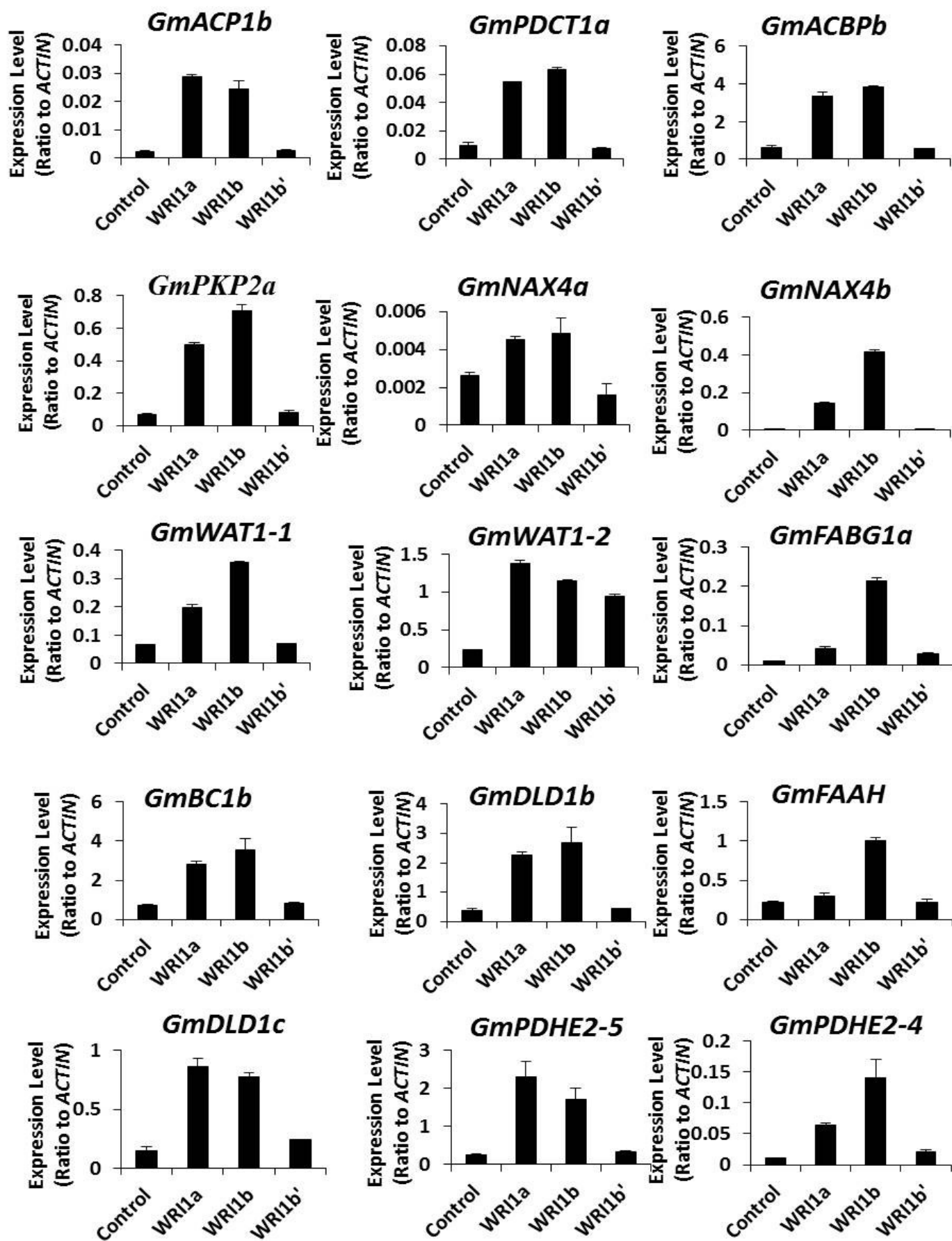


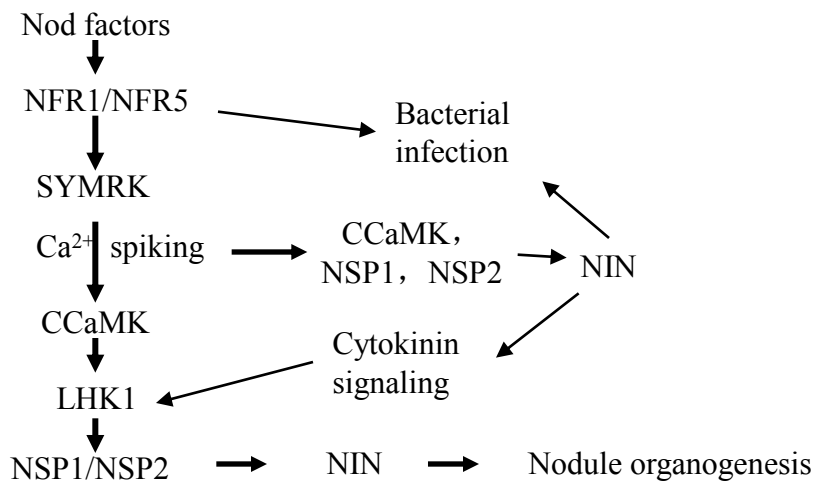
Figure S7. Quantitative PCR confirmation of gene regulation by GmWRI1 in soybean hairy roots.

ACP1b:Glyma15g098500 (Glyma15g10520)
PDCT1a:Glyma08g213100 (Glyma08g22750)
ABCPb:Glyma09g214500 (Glyma09g34770)
PKP2a:Glyma09g126300 (Glyma09g23150)
Annexin-like protein RJ4(NAX4)
NAX4a:Glyma13g199500 (Glyma13g26960)
NAX4b:Glyma11g153800 (Glyma11g21480)
WAT1-1: Glyma19g173800 (Glyma19g35720)
WAT1-2:Glyma04g251000 (Glyma04g43000)
FABG1:3-oxoacyl-[acyl-carrier-protein] reductase 1
FABG1a:Glyma11g248000 (Glyma11g37320)
BC:Biotin carboxylase 1
BC1b:Glyma08g027600(Glyma08g03120)
DLD1:Dihydrolipoyl dehydrogenase 1
DLD1b:Glyma17g032300 (Glyma17g03560)
DLD1c:Glyma15g143100 (Glyma15g15310)
PDHE2: Dihydrolipoyllysine-residue acetyltransferase component of pyruvate dehydrogenas
PDHE2-5:Glyma10G215400 (Glyma10g35960)
PDHE2-4:Glyma.20g176300 (Glyma20g24830)
FAAH:Fatty acid amide hydrolase
FAAH:Glyma08g003100 (Glyma08g00535)

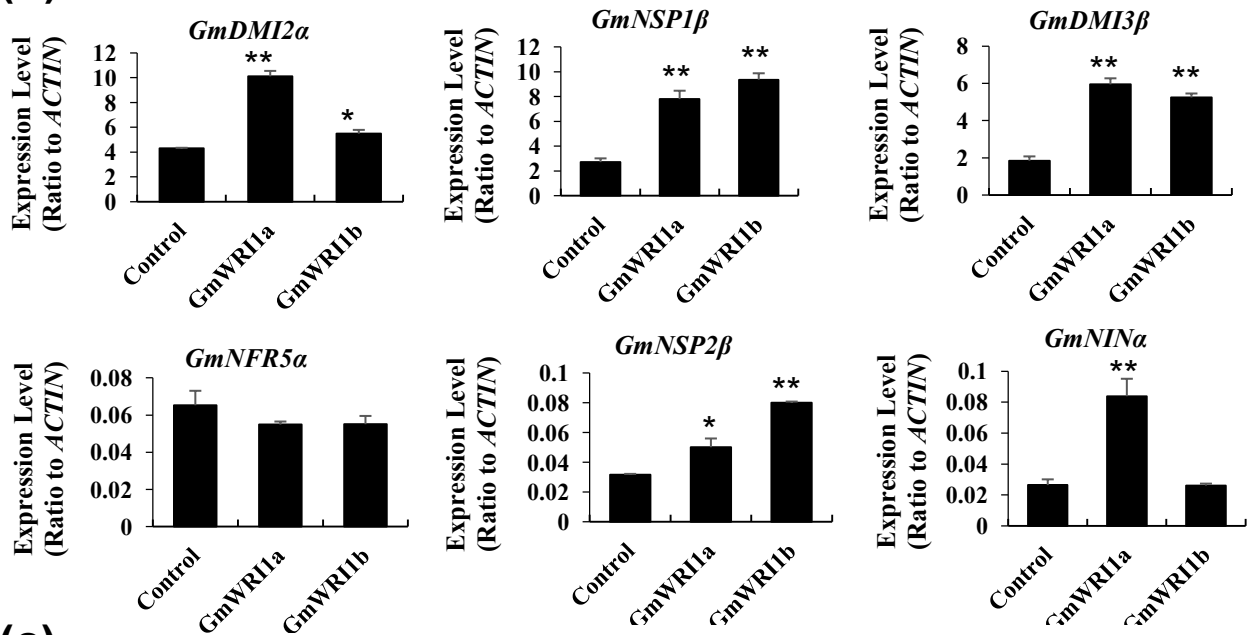
All data are expressed as mean \pm SD from at least three biological duplicates. * $P < 0.05$ and ** $P < 0.01$ by Student's *t* test for significant difference.

Figure S8

(a)



(b)



(c)

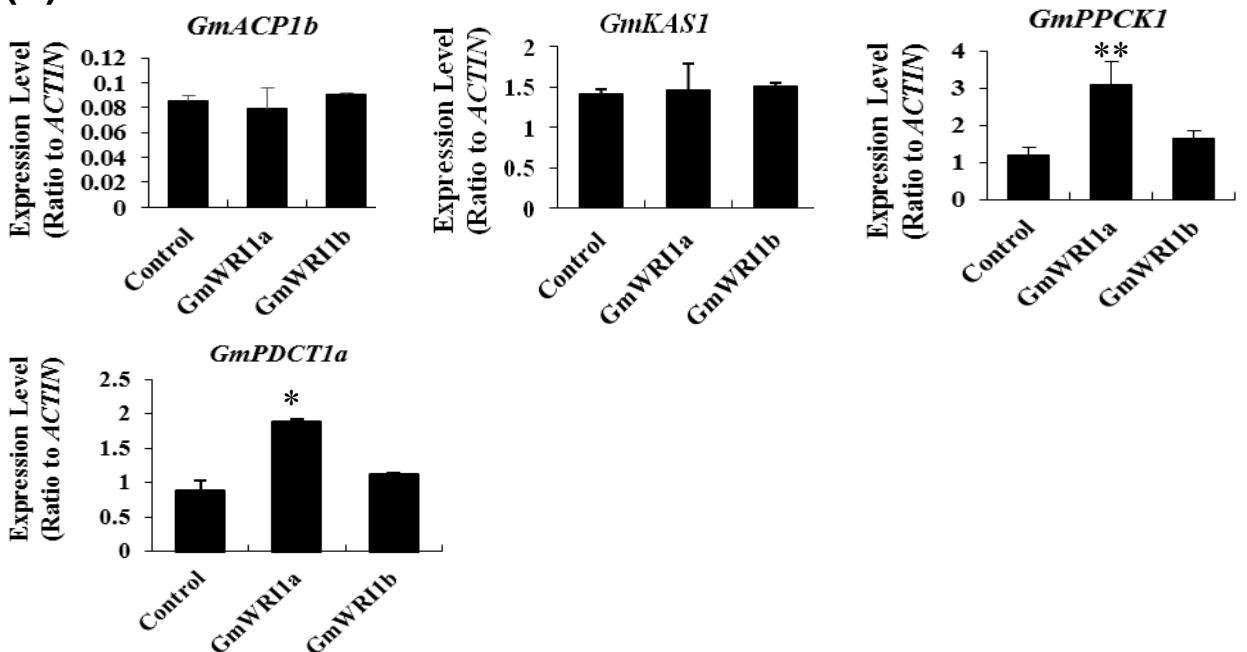
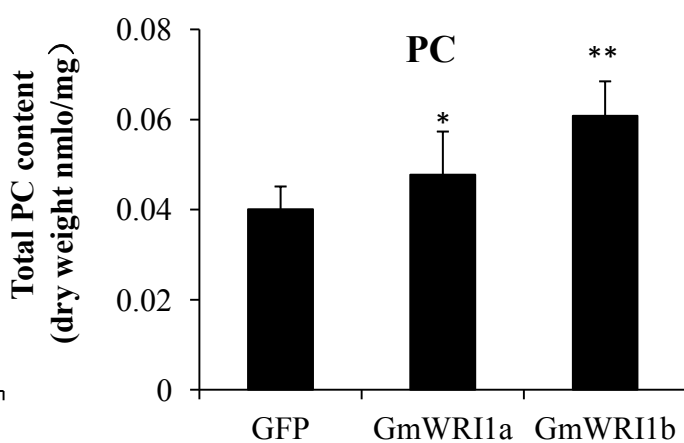
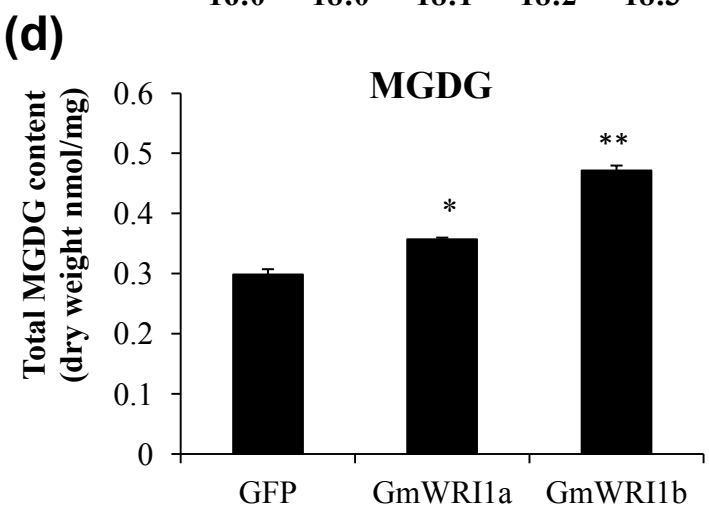
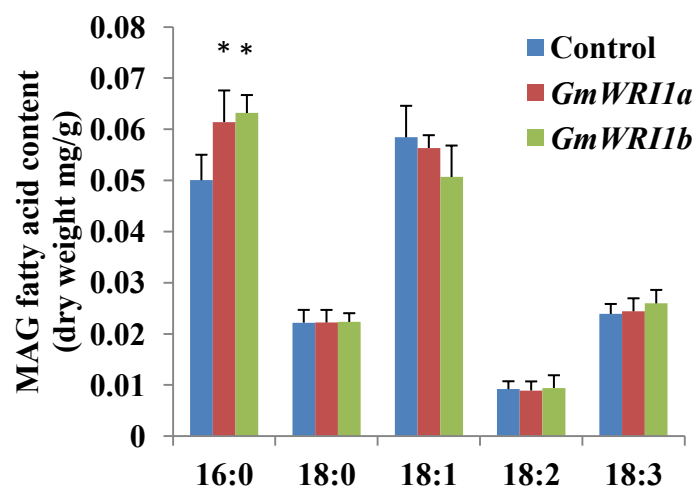
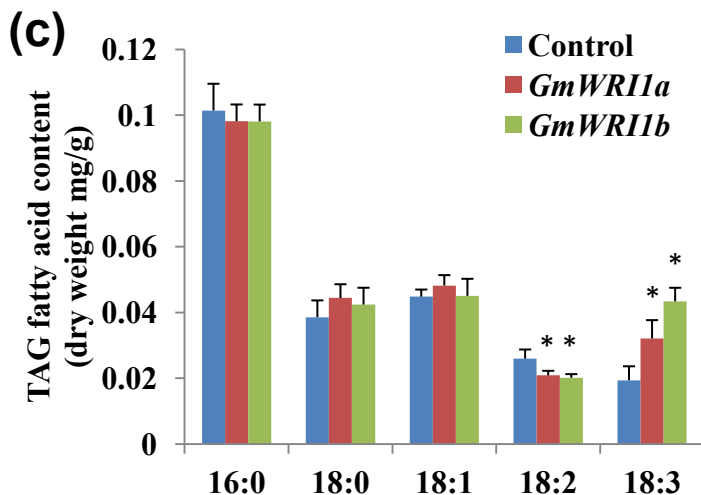
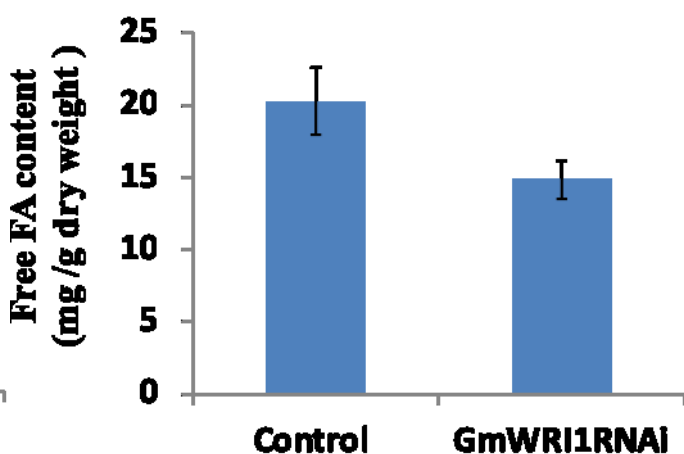
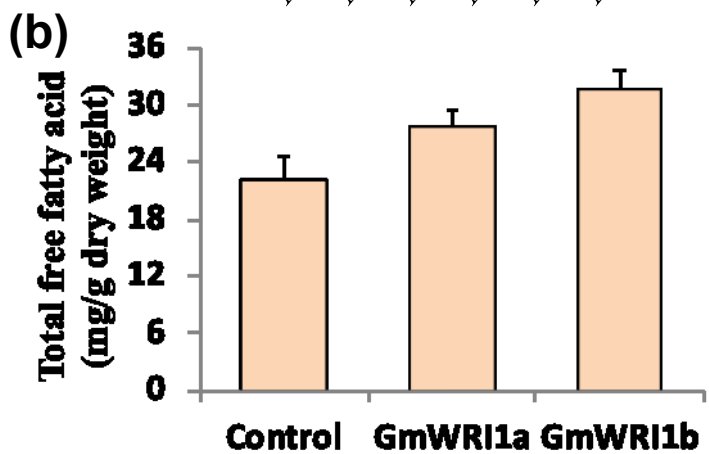
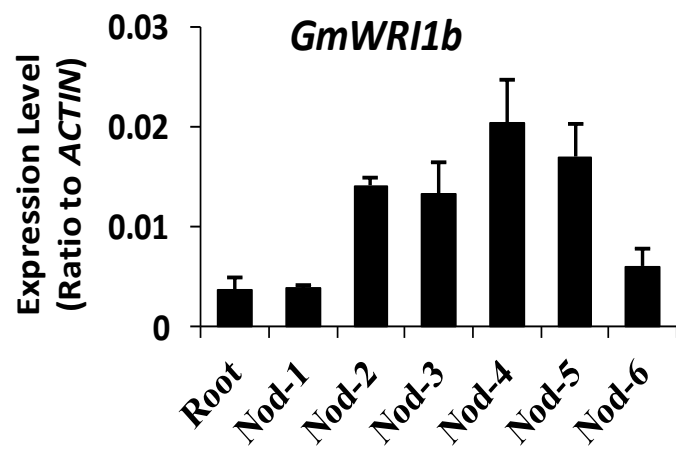
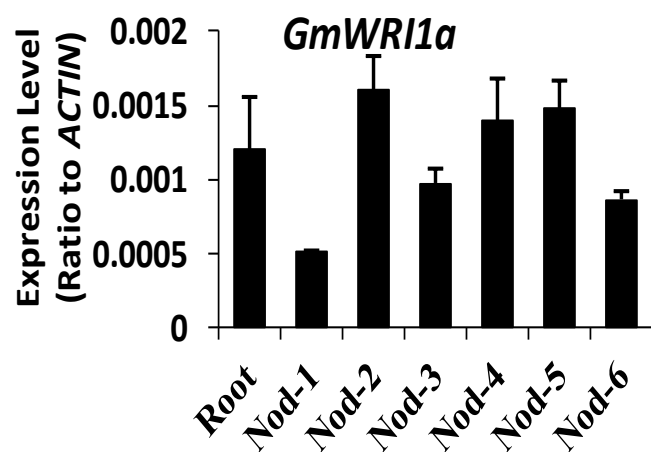


Figure S8. Effects of *GmWRI1a* and *b* overexpression on soybean nodulation and glycolysis and lipid metabolism.

- (a) Schematic of nodulation signal pathway.
- (b) qRT-PCR verification of expression levels of early nodulation genes.
- (c) qRT-PCR verification of expression levels of glycolysis and lipid metabolism gene.

All data are expressed as mean \pm SD from at least three biological duplicates. * $P < 0.05$ and ** $P < 0.01$ by Student's *t* test for significant difference.

Figure S9**(a)**

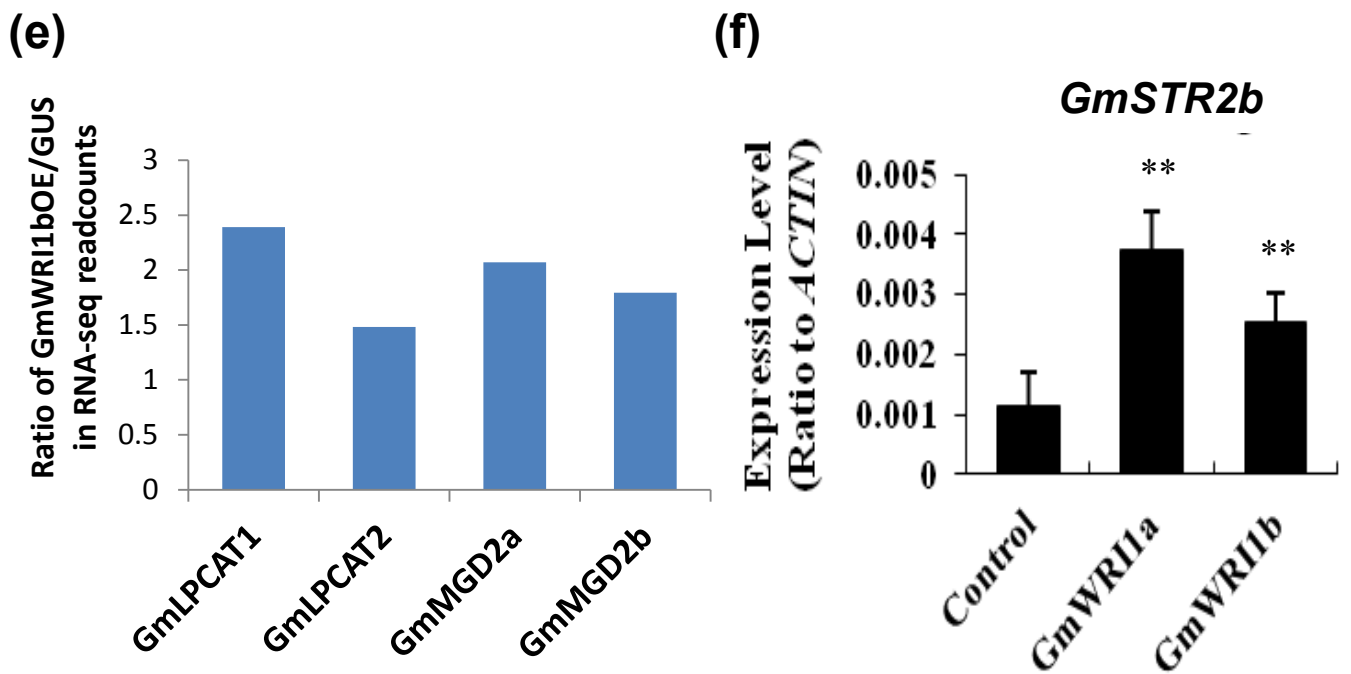
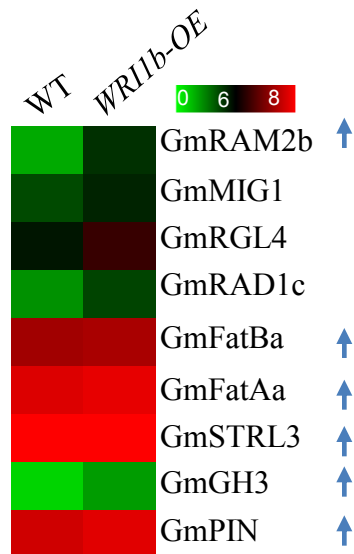
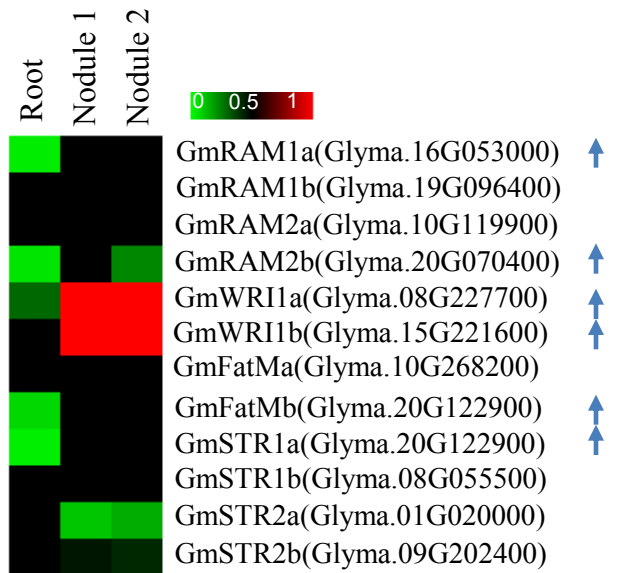
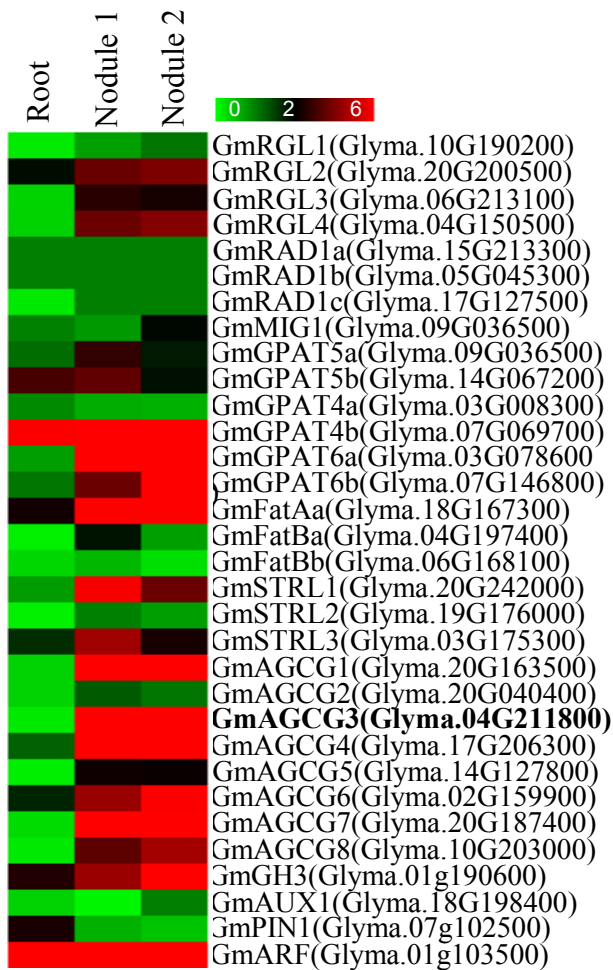


Figure S9. Accumulation of lipids and expression patterns of soybean lipid synthesis –related genes at soybean nodule developmental stages.

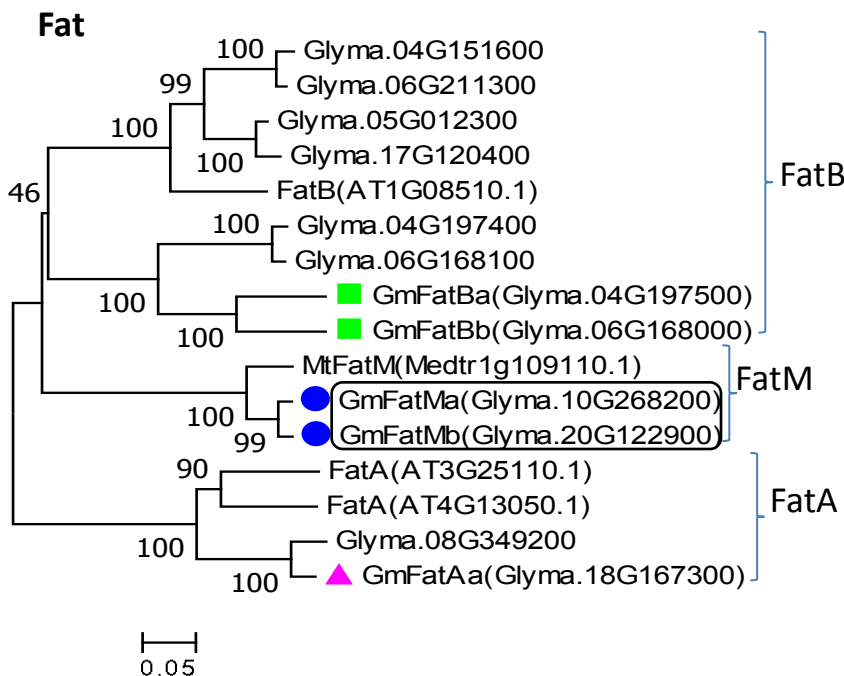
- (a) qRT-PCR analysis of *GmWRI1* expression.
- (b) Contents of free fatty acids in soybean nodules of *GmWRI1a* or *b*-overexpressing and *GmWRI1RNAi* hairy roots, as compared with these nodules from *GUS*-expressing hairy roots (as a control).
- (c) Fatty acid contents in TAGs and MAGs from nodules overexpressing *GmWRI1a* and *GmWRI1b*.
- (d) Total MGDG and PC contents in the nodules overexpressing *GmWRI1a* and *GmWRI1b*.
- (e) Up-regulation of PC and MGDG synthesis genes lysophosphatidylcholine acyltransferase 1 (LPCAT1)(Glyma17g14070) and LPCAT2(Glyma05g03510) and Type B MGDG synthase 2a (MGD2a) (Glyma17g11720) and GmMGD2b (Glyma13g23150) in GmWRI1b OE hairy roots as compared with GUS control.
- (f) qRT-PCR verification of expression levels of lipid transporter gene GmSTR2b (Glyma09G202400).

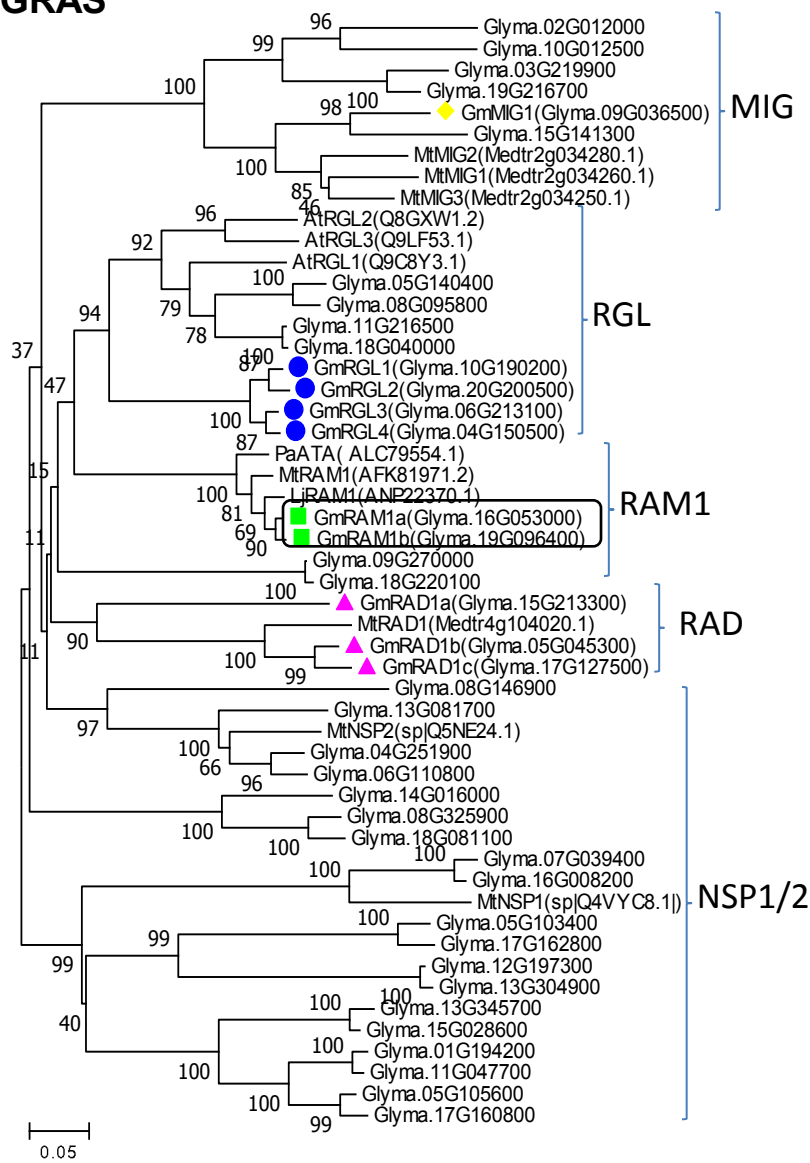
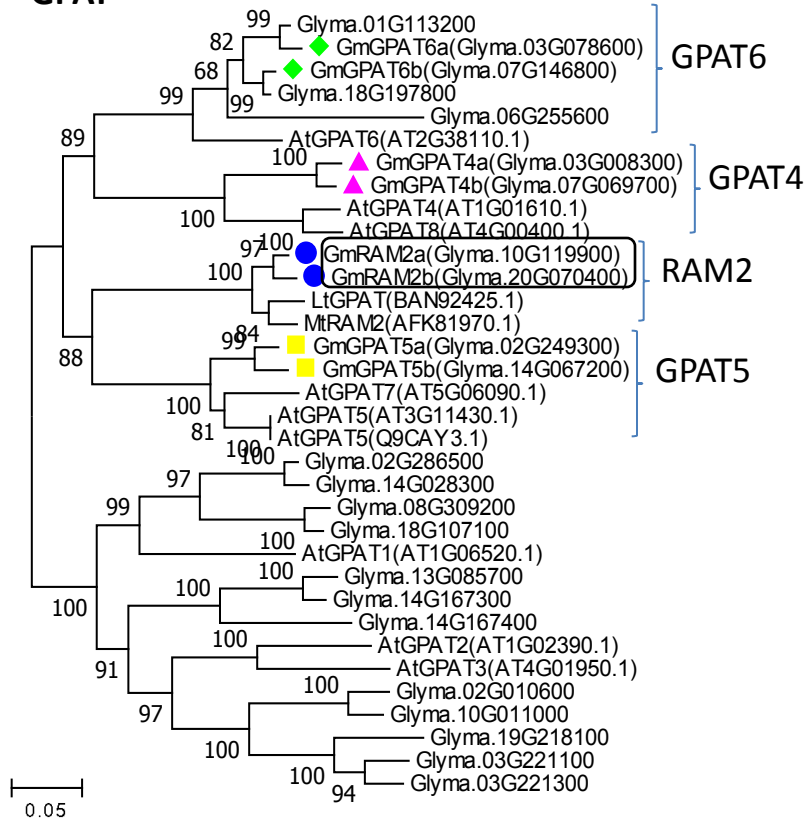
Figure S10

(a) (b)



(c)



(d)**GRAS****(e)****GPAT**

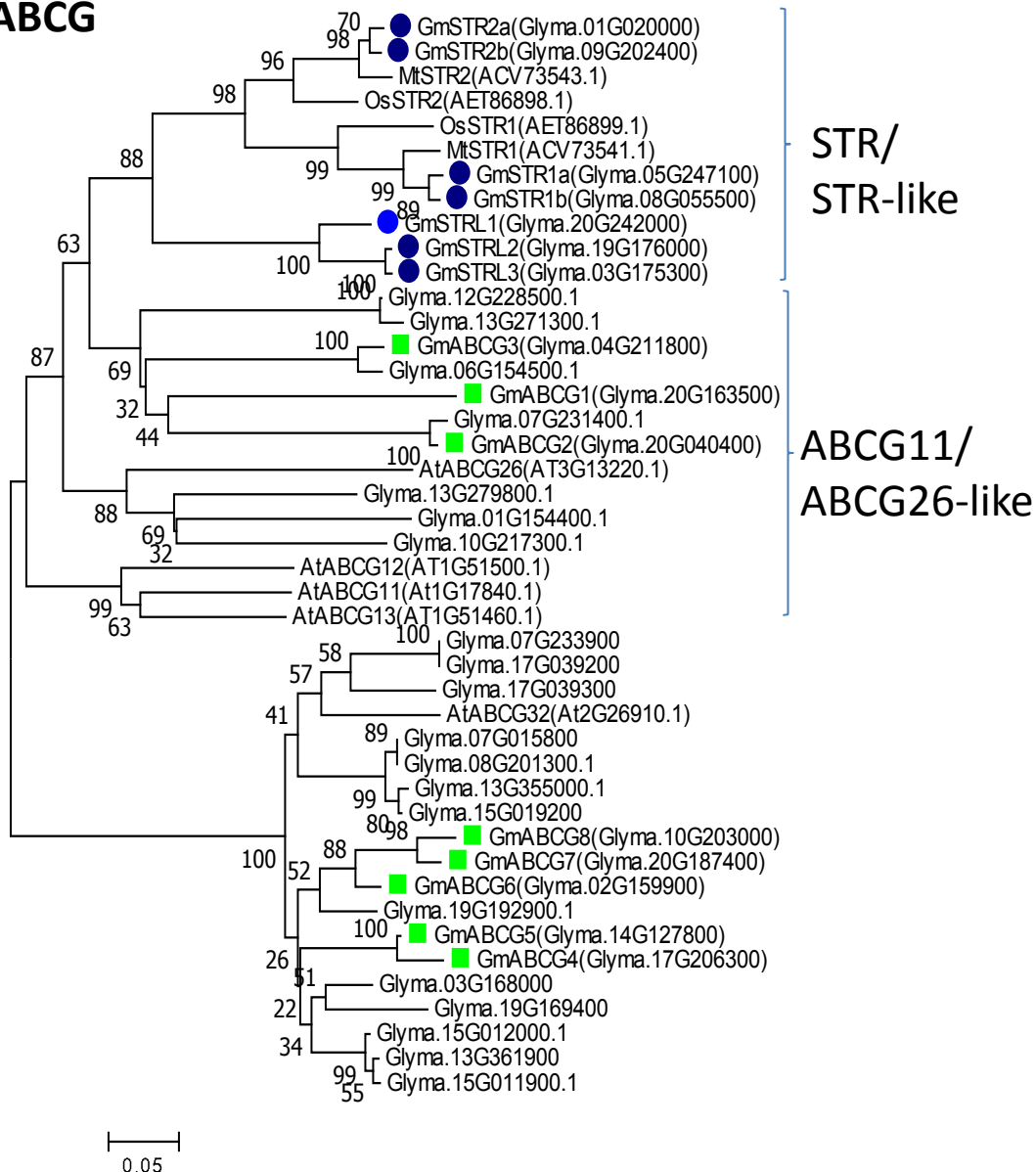
(f)**ABCG**

Figure S10. Identification and transcriptional analysis of FatB, GPAT, GRAS transcription factors RAM1 and ABCG transporter STR1/2.

(a) Heatmap analysis of soybean homologue genes for Medicago RAM1, RAM2, WRI1, STR, and FatM.

(b) Expression of ortholog genes (g) for *M. truncatula* RAM1, RAM2, WRI1, STR1/2, and FatM in root and nodule and genes with WRI1-binding cis-elements related to auxin modification, transport, signaling, or 2-MAG synthesis or transport in WT and *GmWRI1bOE* line.

(c) Phylogenetic identification of soybean FatB and FataA genes homology to Medicago and Lotus or other fatty acyl binding protein thioesterase (Fat)

(d) Phylogenetic identification of soybean GRAS genes homology to Medicago and Lotus or other GPATs.

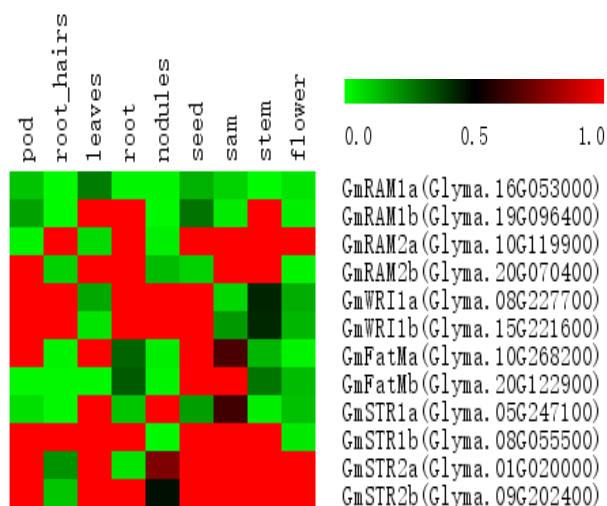
(e) Phylogenetic identification of soybean GPAT genes homology to Medicago and Lotus or other GPATs.

(f) Phylogenetic identification of soybean ABCG transporter genes homology to Medicago and Lotus or other STR1/2 or lipid transporters ABCG11, ABCG26 . .

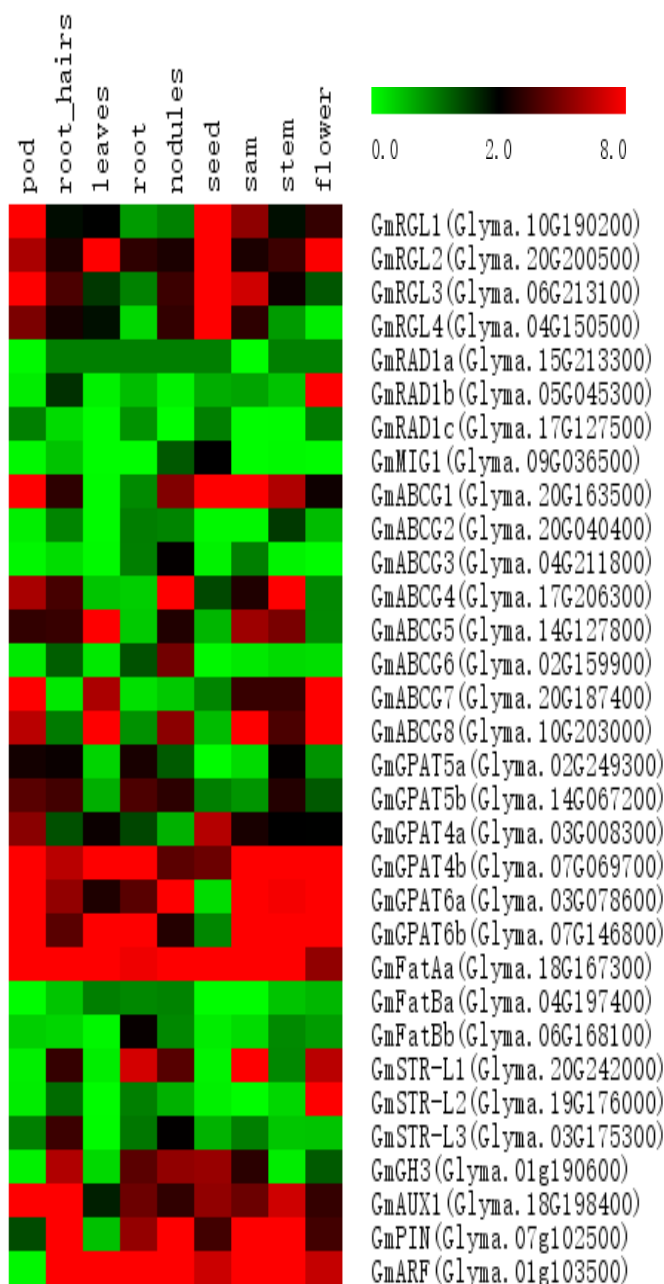
The alignment was generated using Clustal W and the unrooted phylogram was constructed with MEGA6 software using the neighbor-joining method.

Figure S11

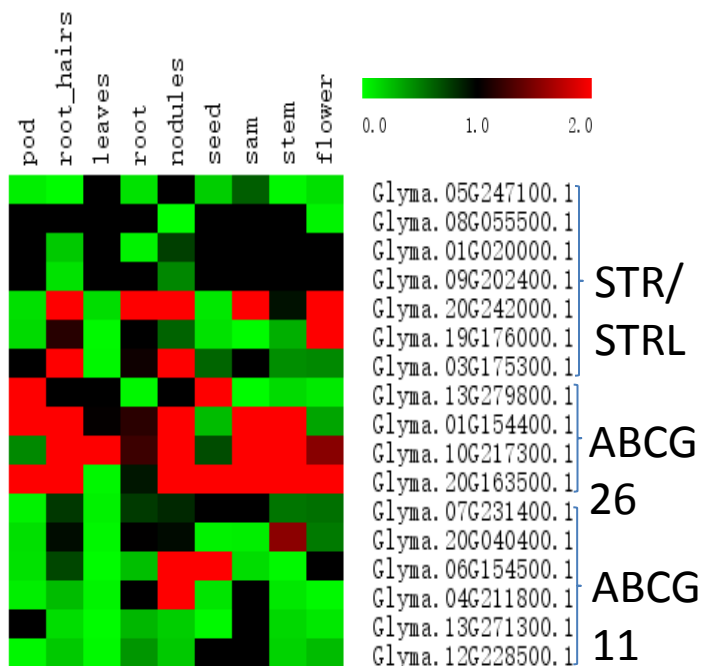
(a)



(b)

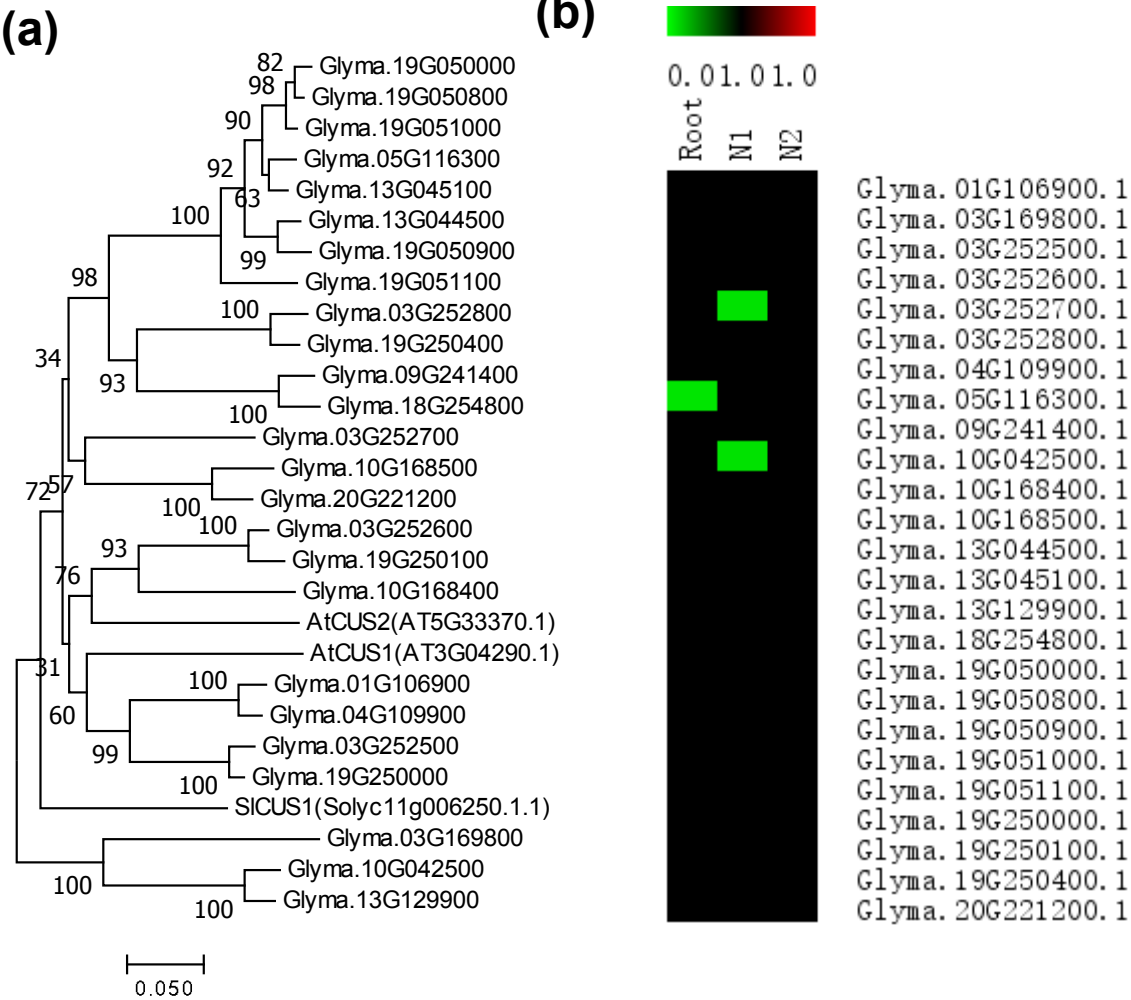


(c)



Supplemental figure S11. The heat map analysis of tissue expression patterns of ortholog genes (a), other homology genes (b) for *M. truncatula* RAM1, RAM2, WRI1, STR1/2, and FatM. (c) is the tissue expression of ABCG11, ABCG26, RGL, RAD, and STR-like (STRL).

Figure S12



Supplementary figure12. The phylogenetic tree (a) and heat map analysis (b) in roots and nodules of CUS (cutin synthase). The alignment was generated using Clustal and the unrooted phylogram was constructed with MEGA6 software using the neighbor-joining method. The heat map was made by MeV software.

Figure S13

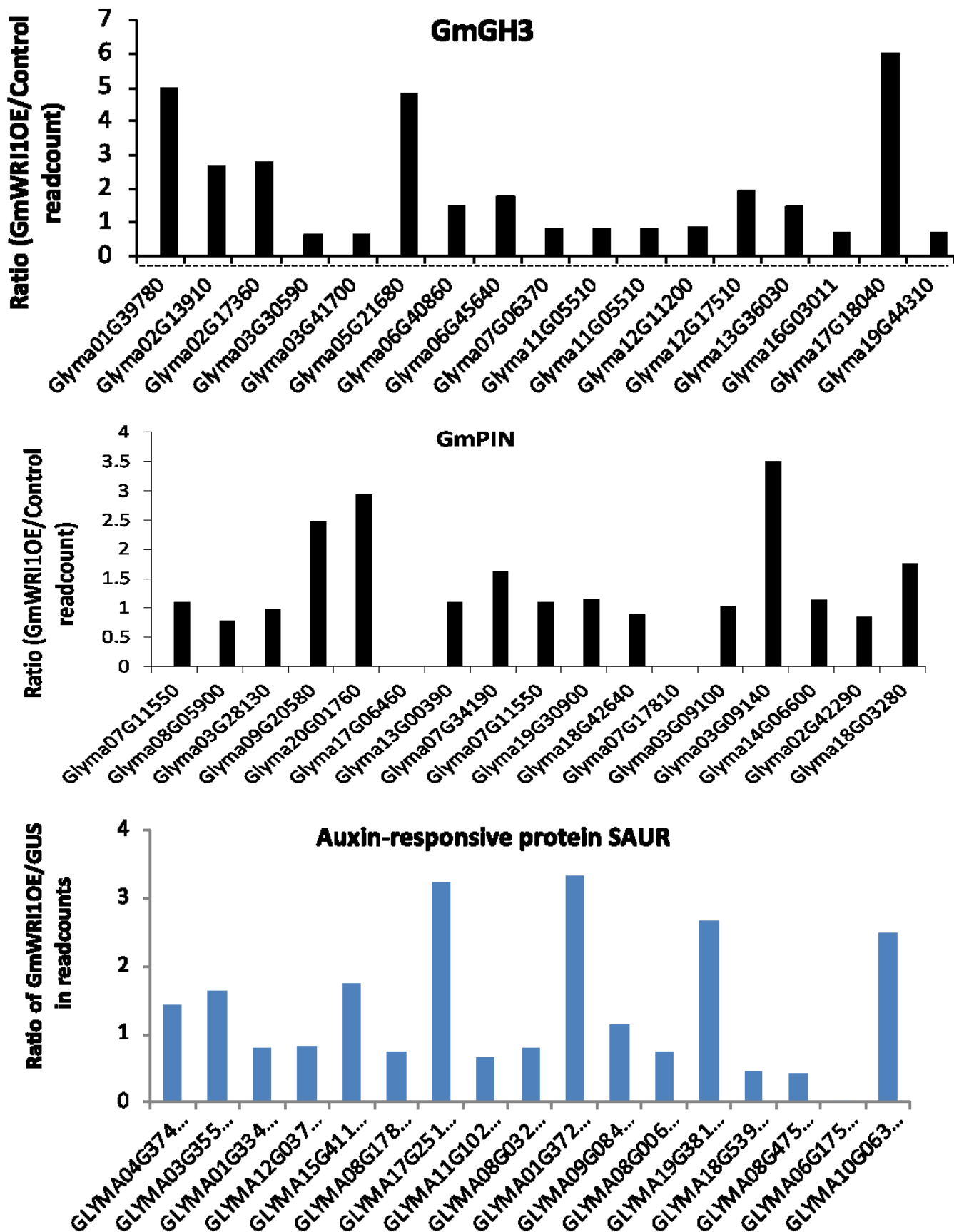


Figure S13. Expression level of *GmGH3*, *GmPIN*, and *Auxin-responsive protein SAUR* genes in *GmWRI1b* overexpression (*GmWRI1bOE*) hairy roots, as compared with control (*GUS*) hairy roots.

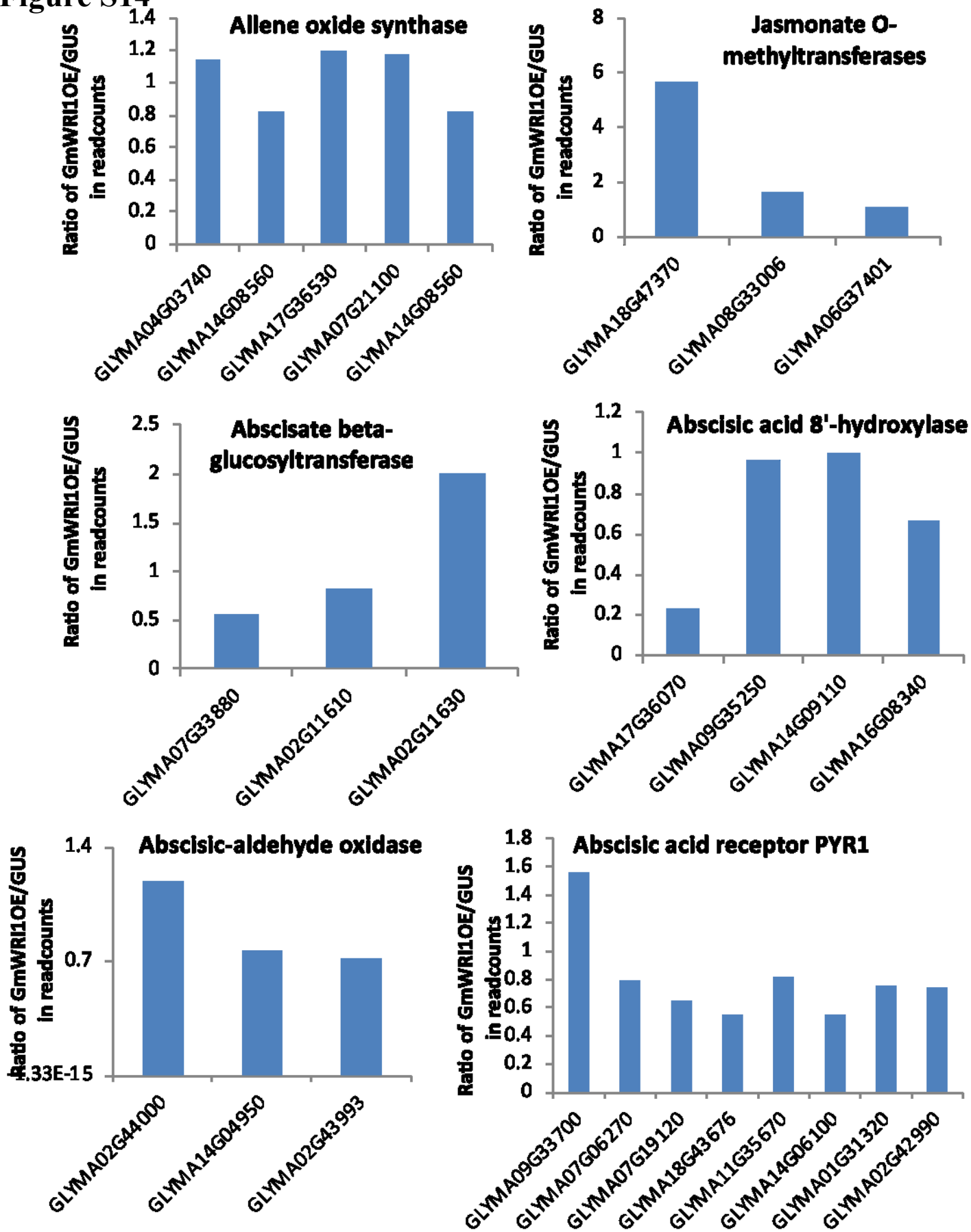
Figure S14

Figure S14. Expression level of jasmonate biosynthesis and abscisic acid biosynthesis and catabolic genes in *GmWRI1b* overexpression (*GmWRI1bOE*) hairy roots, as compared with control (*GUS*) hairy roots.

Figure S15

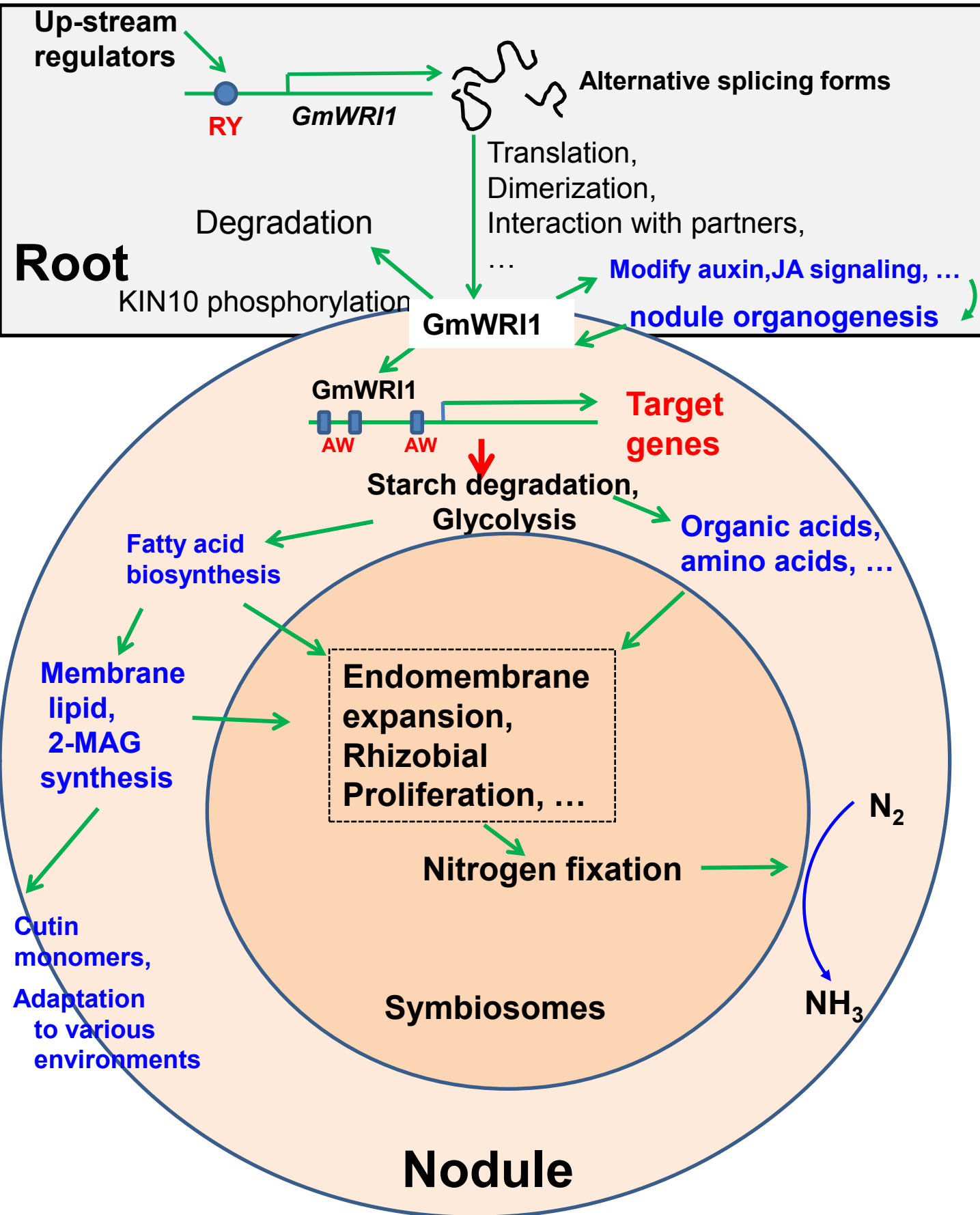


Figure S15. Proposed functions for GmWRI1s in soybean nodulation